Author Manuscript

Author Manuscript

Author Manuscript

Author Manuscript

HHS Public Access

Author manuscript

Nat Neurosci. Author manuscript; available in PMC 2012 March 01.

Published in final edited form as:

Nat Neurosci. ; 14(9): 1135–1141. doi:10.1038/nn.2870.

Acute destruction of the synaptic ribbon reveals a role for the ribbon in vesicle priming

Josefin Snellman[1], **Bhupesh Mehta**[1], **Norbert Babai**[4], **Theodore M. Bartoletti**[4], **Wendy Akmentin**[5], **Adam Francis**[1], **Gary Matthews**[5], **Wallace Thoreson**[4], and **David Zenisek**[1,2,3]

[1]Department of Cellular and Molecular Physiology, Yale University School of Medicine, New Haven, CT 06520

[2]Department of Ophthalmology and Visual Sciences, Yale University School of Medicine, New Haven, CT 06520

[3]Center for Cellular Neuroscience, Neurodegeneration and Repair, Yale University School of Medicine, New Haven, CT 06520

[4] Dept. of Ophthalmology & Visual Sciences, University of Nebraska Medical Center, Omaha, NE 68198

[5]Department of Neurobiology and Behavior, Stony Brook University, Stony Brook, NY 11794

Abstract

In vision, balance, and hearing, sensory receptor cells translate sensory stimuli into electrical signals whose amplitude is graded with stimulus intensity. The output synapses of these sensory neurons must provide fast signaling to follow rapidly changing stimuli, while also transmitting graded information covering a wide range of stimulus intensity and sustained for long time periods. To meet these demands, specialized machinery for transmitter release—the synaptic ribbon—has evolved at the synaptic outputs of these neurons. Here we show that acute disruption of synaptic ribbons by photodamage to the ribbon dramatically reduces both sustained and transient components of neurotransmitter release in mouse bipolar cells and salamander cones, without affecting the ultrastructure of the ribbon or its ability to localize synaptic vesicles to the active zone. Our results indicate that ribbons mediate slow as well as fast signaling at sensory synapses, and support an additional role for the synaptic ribbon in priming vesicles for exocytosis at active zones.

Users may view, print, copy, download and text and data- mine the content in such documents, for the purposes of academic research, subject always to the full Conditions of use: http://www.nature.com/authors/editorial_policies/license.html#terms

Correspondence and requests for materials should be addressed to D.Z. (david.zenisek@yale.edu).

Author contributions: J.S. conducted experiments for figures 2, 3 and 4 and 6 and analyzed data for figures 2, 3 and 4 and contributed to the editing and the writing of the manuscript, B.M. performed experiments and analysis for figure 3, M.B., T.M.B. and W.B.T. performed and analyzed experiments for figure 5, W.B.T. also contributed to the editing and writing of the manuscript. W.A. performed electron microscopy for figure 6 and supplemental figures, A.F. performed experiments for figure 1. G.M. oversaw electron microscopy experiments and edited and contributed to the writing of the manuscript. D.Z. prepared the manuscript, oversaw the project, performed experiments for figure 1 and performed the analysis for figures 1 and 6.

Author Manuscript Author Manuscript Author Manuscript Author Manuscript

Introduction

Neurons communicate with each other primarily via synaptic contacts where chemical neurotransmitters are released. Transmitter-containing vesicles undergo a series of steps that ultimately lead to their fusion with the presynaptic plasma membrane, including trafficking to the active zone, docking with the membrane, and a priming step that readies vesicles for fusion. At most synapses, vesicle fusion is precisely timed to the occurrence of a presynaptic action potential[1], resulting in a fast, transient burst of release. However, in addition to transient release, synaptic transmission at sensory neurons of the vertebrate visual, auditory, and vestibular systems also occurs by continuously graded modulation of ongoing neurotransmitter release. These cells have evolved specific structures, known as synaptic ribbons, for this task[2]. Ribbons are proteinaceous structures that extend into the cytoplasm at the active zone and are surrounded by a halo of synaptic vesicles tethered to the ribbon by fine filaments[3]. Vesicles at the base of the ribbon are docked at the plasma membrane, poised to provide fast transient release when calcium channels open, while the more distal vesicles might support the continuous mode of release characteristic of ribbon-type synapses. However, whether ribbons operate in this fashion is unknown, and even if they do, it is not clear if the ribbon acts as a simple depot for vesicles, or plays a more active role. In addition, the basic notion that ribbons are important for sustained release has been called into question[4].

Genetic manipulations present from birth may allow for developmental compensation and/or changes in synaptic transmission arising from homeostatic mechanisms[5]. To address the role of the ribbon in synaptic transmission, we chose to acutely damage the ribbon while monitoring synaptic transmission. We find that immediately after damage to the ribbon, one can evoke a burst of release that is relatively unchanged. However, after depleting a releasable pool with an initial stimulus, both rapid and sustained components of release were disrupted by ribbon damage. Retrospective electron microscopy revealed a normal complement of vesicles on the ribbon in damaged ribbons after depletion of the resistant pool. Together, these data suggest a role for the ribbon in preparing vesicles for exocytosis, subsequent to vesicle tethering to the ribbon.

Results

Fluorophore-assisted light inactivation of the synaptic ribbon

To investigate potential roles for the synaptic ribbon in exocytosis, we used fluorophore-assisted light inactivation (FALI)[6,7] to acutely disrupt the ribbon, while monitoring neurotransmitter release in paired pre- and postsynaptic recordings. FALI takes advantage of singlet oxygen generated upon excitation of fluorescent molecules to generate local damage, with half-maximal damage occurring within ~40 Å of the fluorophore[7]. To specifically target the synaptic ribbon, we used a whole-cell patch pipette to introduce a fluorescein-labeled short (14 amino acid) peptide containing a “PXDLS” peptide sequence that binds to the CtBP domain of the most abundant protein in the synaptic ribbon, ribeye[8]. Previous work has demonstrated that fluorescently-tagged peptides containing this motif effectively target to synaptic ribbons in several preparations[8-12], including the two preparations used here, the mouse rod-bipolar cell[10] and the salamander cone photoreceptor[12]. As expected,

Author Manuscript Author Manuscript Author Manuscript Author Manuscript

introduction of the fluorescently labeled peptide effectively labeled punctate structures consistent with ribbons in the synaptic terminal regions of both mouse rod bipolar cells (Fig. 1a) and salamander cones (Fig. 1b).

We hypothesized that photodamage induced by illumination might manifest as a decrease in the ability of the ribbon to bind to the peptide due to destruction of the ribeye protein. To test this idea, dissociated mouse bipolar cells were whole-cell voltage clamped with a solution containing the fluorescein-conjugated ribbon binding peptide. As seen in Figure 1c, mouse bipolar cells loaded with the peptide exhibited fluorescent spots in the synaptic terminal, denoting the location of synaptic ribbons[10]. Next, bipolar cell terminals were exposed to continuous 488 nm laser illumination for 15 seconds to photobleach fluorescein conjugated peptides within the synaptic terminal. Afterward, both the spot and cytoplasmic fluorescence dimmed as expected. After a period of 150 seconds, the fluorescence returned to pre-bleach levels within the cytoplasm as unbleached peptide replaced bleached peptide. Despite the return of fluorescence to the cytoplasm, spot fluorescence did not recover (figure 1c, right), consistent with damage to ribeye.

Since the lack of recovery from photobleaching could conceivably result from a stable association between ribeye and the non-fluorescent peptide, we sought to estimate how fast the peptide unbinds from the ribbon. To do so, dissociated mouse bipolar cells were superfused with a solution containing the detergent β-escin to permeabilize the plasma membrane and allow access of the peptide to the ribbons inside the cell. After detergent treatment, bipolar cells were locally superfused with a solution containing 50 μM of the ribbon-binding peptide conjugated to the fluorophore HyLite 488 for 10-15 seconds. Upon application of the fluorescent peptide, spots became visible in the permeabilized synaptic terminal (figure 1d; t = 0s). Next, we washed with peptide-free solution and monitored spot fluorescence at 2 second intervals to estimate the unbinding rate from the ribbon. The fluorescence decay during the washing period was roughly exponential with a time constant of 14.7 s (Fig. 1e). A second application exhibited similar intensity spots to the first (87 ± 9 % of first application), indicating that the fluorescence decay was not due to photobleaching. Of note, the speed of superfusion and exit of fluorescent peptide from the permeabilized cell may limit the rate of fluorescent decrease in these measurements. Therefore, the apparent off-rate measured here may be slower than the actual unbinding rate. Despite these limitations, the off-rate measured here is too fast to account for the FRAP results above, indicating that photobleaching of the ribbon-binding peptide damages the peptide binding site of ribeye.

Acute ribbon damage alters synaptic release from rod bipolar cells

To investigate the role of the synaptic ribbon in synaptic transmission, we next used photobleaching of the ribbon-binding peptide to selectively damage ribbons in paired whole-cell voltage clamp recordings of retinal neurons. Specifically, we recorded pre-synaptically from mouse rod bipolar cells, while simultaneously monitoring the postsynaptic response of AII amacrine cells. Rod bipolar cells form multiple (6 to 10) glutamatergic synapses with postsynaptic AII-amacrine cells[13,14]. In response to 100 ms step depolarizations to 10 or 0 mV from a holding potential of 60 mV, excitatory post synaptic currents (EPSCs) recorded

Author Manuscript Author Manuscript Author Manuscript Author Manuscript

from AII amacrine cells exhibited two temporal components of release: a fast synchronous component followed by a slower asynchronous component, as previously described[15,16]. Importantly, neither receptor desensitization nor receptor saturation have much impact on the kinetics of the responses at this synapse[15-18]. Based on the size and rapidity of the fast kinetic component, this component likely arises from docked and primed vesicles found at the base of the synaptic ribbon[13,19].

We tested whether the ribbon-binding peptide alone had any effect on the amount or time course of synaptic release. The peak EPSC evoked by presynaptic depolarization averaged 134.0 ± 12.7 pA (n=10) in the presence of the peptide and 138.5 ± 14.8 pA (n=5) when recorded without the peptide in the presynaptic cell (Fig. 2a). To analyze the kinetics of the synaptic response, we integrated the postsynaptic response over time and fit the resultant curves with a double exponential function:

$$Q(t)=A_1e^{-t/\tau 1}+A_2e^{-t/\tau 2} \quad (1).$$

Synaptic currents recorded in response to 100-ms steps to −10 mV were well fit by this function (Fig. 2b). On average, the best fit values for A_1, A_2, τ_1 and τ_2 were 1.0821 pC ± 0.24043, 10.041 pC ± 2.183, 8.022 ms ± 2.501 and 309.56 ms ± 87.651, respectively, in control cells lacking the peptide (n=10). The values of the fit parameters were not significantly different in cells loaded with 40 μM fluorescent ribbon-binding peptide (Fig. 2c; n = 6 pairs). The charge of a spontaneous mEPSC was on average 40.6 fC, making the size of A_1 and A_2 equivalent to 26.7 and 247 vesicles, or 4.4 and 41 vesicles per ribbon, assuming 6 synaptic ribbons connecting each bipolar cell to each AII amacrine cell[14]. Evidently, the synaptic ribbon-binding peptide has no effect on the time course, magnitude, or repeatability of the synaptic current.

Next, bipolar cells were loaded with 10 - 40 μM ribbon-binding peptide or with 40 μM of a scrambled control peptide. Cells were depolarized to −10 or 0 mV for 100 ms every 60 seconds, while neurotransmitter release was monitored post-synaptically. After 4 depolarizations, bipolar cells were illuminated with bright blue light for 15 seconds to photobleach fluorescein and generate local damage near the peptide. Figure 3a–c shows an example of one of these experiments. In the first response following exposure to bleaching light (Fig. 3b), EPSCs exhibited near normal peak responses, a reflection of the fast component of vesicle release. In subsequent responses (Fig. 3c), both fast and sustained components were substantially reduced, with no change in the size of the presynaptic calcium current (inset). Of note, photobleaching the ribbons also eliminated the presynaptic glutamate transporter current in bipolar cells[16,20], which can be observed as a deviation from the expected square wave for the calcium current. This is likely due to presynaptic calcium current rather than proton block of the calcium current [21-23], because the transporter blocker *threo*-β-benzyloxyaspartate blocked the effect, whereas manipulation of extracellular buffering did not (data not shown). This is consistent with the strong reduction in postsynaptic response (arrows Fig. 3a–c inset). Photobleaching the scrambled peptide affected neither EPSCs (Fig. 3d) nor presynaptic calcium current. Even with intervals of 5 minutes between stimuli, synaptic responses exhibited little recovery (Fig. 3e; see online

Author Manuscript Author Manuscript Author Manuscript Author Manuscript

methods for details). In 4 cells where longer delays were tested, epsc amplitudes were reduced to 31.5 ± 5.9 % of the pre-bleach epscs in the 5th response after photobleach and 29.6 ± 6.9 % after a 5 minute delay. These results indicate that acute damage to the ribbon nearly eliminates neurotransmitter release, but that a pool of releasable vesicles is initially spared from ribbon damage.

Figure 3f examines the relation between concentration of the peptide and the reduction in neurotransmitter release in the second response after light exposure. The effect on both the synchronous and delayed components exhibited similar concentration dependence, with half maximal suppression between 5 and 10 μM. Of note, the concentration dependence is similar to the measured affinity of this peptide for ribbons in goldfish bipolar cells (27 μM)[8] as well as the affinity of this peptide sequence *in vitro* for CtBP1 (1.5 μM) [24], a protein with high homology to the b-domain of ribeye[25].

Figure 4 examines the kinetics of synaptic response for the pool of releasable vesicles that was initially resistant to photodamage. Figure 4a shows the average epscs for one bipolar-Aii pair before (gray), first after photobleach (red) and subsequent responses after photobleach (black). To compare the kinetics of the response before and in the first response after photobleach, the time integrals of the EPSCs are plotted together in Figure 4b for cells loaded with the ribbon-binding peptide and in Figure 4c for the scrambled peptide control. We fit the charge as a function of time to equation (1) for the recordings before photobleach. After photobleach, we fit the charge with equation (1) while keeping the time constants fixed to estimate the effect of ribbon damage on both fast and slow components of release. Photodamage to the ribbon reduced the amplitude of the slow component, A_2, by 43% immediately after photobleach and A_1 by 22%. In subsequent responses, both components were greatly attenuated, A_1 by 71%, and A_2 by more than 78%. Evidently, damage to the synaptic ribbon allows one-time release of a single pool of vesicles, but refilling of this pool is prevented, consistent with a role just upstream of the final fusion event. If we measure the photo-damage resistant pool size as the difference between the first response after photobleach and the subsequent responses, we get a pool size equivalent to 200 vesicles.

As shown in Figure 4, a small amount of release remained after photobleach and a stimulus. This residual release could result from undamaged ribbon proteins or from extraribbon release sites. To distinguish between these two possibilities, 6 bipolar cells were subjected to a second light stimulus after allowing for sufficient time to reload the synaptic terminal with fluorescent peptide. On average the second photobleach decreased the residual release with A_1 decreasing by 63.6 ± 16% and A_2 by 87.8 ± 8.7 %. These results indicate that the residual release was also sensitive to photodamage from illumination of the ribbon-binding peptide, consistent with a ribbon requirement for synaptic communication between rod bipolar cells and AII amacrine cells. Figure 4c shows control responses before and after photobleach for cells loaded with a scrambled version of the peptide.

Acute ribbon damage alters release but not endocytosis in cones

To determine if the above findings can be generalized to other ribbon synapses, we next tested whether a different ribbon-type presynaptic terminal, the cone photoreceptor of the tiger salamander, exhibited a similar response to photodamage of ribbons. To do so, we

Author Manuscript Author Manuscript Author Manuscript Author Manuscript

recorded presynaptically from cones loaded with the fluorescein-conjugated peptide while simultaneously monitoring postsynaptic responses in synaptically connected off bipolar cells or horizontal cells. Similar to bipolar cells, cone photoreceptors exhibit at least two distinct components of neurotransmitter release in response to strong depolarizations, a rapid component that represents release of the rapidly releasable pool and gives rise to a peak in the EPSC, followed by a slower component (Fig. 5a)[11]. After 5 presynaptic depolarizations delivered at 60 s intervals, cones were subjected to 60 seconds of continuous 488 nm illumination to induce ribbon damage. Illumination of the ribbon-binding peptide (Fig. 5a, b), but not scrambled peptide, left both the fast component and the slow component largely intact in the first response after photobleach, with no effect on the presynaptic calcium current (Fig. 5a, inset). In subsequent responses, neurotransmitter release was significantly attenuated (Fig. 5b). Fitting EPSC charge transfer with equation 1 showed that fast and slow components were reduced by 56.9 ± 7.9% and 41.5 ± 8.0% (N=18), respectively. Similar to what was observed in bipolar cells, these values did not differ significantly from one another (P=0.2, paired t-test).

The B-domain of ribeye has high sequence homology to the CtBP3/BARS, a protein with a suggested role in dynamin-independent endocytosis[26]. The cone photoreceptor preparation also allowed us to measure endocytic rates using membrane capacitance measurements to investigate whether photodamage to ribeye affects endocytic rates. Because the membrane capacitance (Cm) is linearly proportional to membrane surface area, the insertion of vesicle membrane during exocytosis causes a net increase in Cm, whereas endocytosis results is marked by a slower recovery to baseline. Cones depolarized to 10 mV for 25 ms exhibited a robust capacitance increase, followed by a slower decay to baseline (Fig. 5c), as previously reported[27]. Prior to photobleach, steps elicited a capacitance jump of 139.1 ± 18.5 fF, whereas after photobleaching capacitance increased by 88.5 ± 12.7 fF (n=12 trials in 8 cells, P=0.0014, paired t-test). We calculated endocytic rate as time required for the capacitance increase to decline by 50% and found no significant difference (P= 0.198, paired t-test) in the $t_{1/2}$ before (121.5 + 22.8 ms) and after (110.2 + 25.1 ms) photobleach. These results indicate that ribbon damage appeared to have no effect on endocytic rate.

Ultrastructure of photodamaged and stimulated ribbons

The above results indicate that damage to the synaptic ribbon blocks resupply of a pool of fast-releasing vesicles. These results could be explained by a failure of new vesicles to reach and dock to release sites or by a failure to prime new vesicles for release. To distinguish between these two models, we performed retrospective electron microscopy to look at vesicle distributions in dissociated mouse bipolar cells in which the ribbon had been photodamaged and then subjected to 2 depolarizations from 60 mV to 0 mV to elicit the depletion of the synaptic response. Figure 6a shows an example of an electron micrograph from a ribbon in a cell which had been loaded with the peptide, voltage clamped, depolarized and exposed to light, whereas Figure 6b shows an example of a control cell which was treated the same way, but without the peptide in the internal solution. More examples are shown in Supplemental Figures 1 and 2. To analyze these data, we counted the number of ribbons and measured their size and the number of vesicles adjacent to the ribbons and determined the number of docked vesicles per ribbon, defined as vesicles whose

Author Manuscript Author Manuscript Author Manuscript Author Manuscript

centers were within 50 nm of the plasma membrane. We found no significant difference in the number of ribbons per total section area(.19 ± .06 ribbons/μm^2 in experimental cells, .22±.07 ribbons/μm^2 in control cells), the size of the ribbons (experimental: 144 ± 21 nm; control: 145 ± 7 nm), the number of vesicles on the ribbon per unit length (experimental: .053 ± .018 vesicles/ nm ribbon; control: .049 ± .004 vesicles/nm ribbon) or the number of docked vesicles per ribbon (experimental: .43 ± .06 vesicles/ribbon section; control: .47 ± .26 vesicles/ribbon section).

In addition, we analyzed EM sections that showed both the synaptic ribbon and the nearby plasma membrane and determined the distance of the vesicles on the ribbon to the plasma-membrane and the number of docked vesicles. Figure 6c shows a cumulative histogram of the distances of vesicles on ribbons to the plasma membrane for both control and cells exposed to both FALI and stimulation. We found no significant difference in vesicle distribution on the ribbon between control and experimental cells.

Lastly, we looked at the size of membrane-bound organelles near the ribbon in control and experimental cells. To do so, we measured the cross-sectional area of all membrane bound organelles within 500 nm from the center of ribbons that were adjacent to the plasma-membrane. On average, we found that the size of organelles were not significantly different ($p = 0.44$; t-test) in control (1299 ± 23 nm^2) and experimental (1329 ± 29 nm^2) conditions. Similarly, a histogram (Fig. 6d) of the distribution of organelle sizes showed no apparent differences between photodamaged and control cells.

Discussion

In this study, we used acute disruption of the synaptic ribbon to investigate potential roles for this structure in neurotransmitter release. Disruption of the ribbon initially left intact a cohort of vesicles that were already prepared for release in both bipolar cells and cones. The size of this photo-damage resistant pool of vesicles had a total charge equivalent to approximately 200 and 45 mEPSCs in bipolar cells and cones, respectively. Using published estimates for the number of synaptic connections between pre and post-synaptic cells, this is equivalent to 25 vesicles per bipolar cell ribbon and 20 vesicles per cone ribbon, similar to the total size of the releasable pool assumed to those that reside on the ribbon [11,28]. Once this resistant pool was depleted, it could not be replenished after ribbons were disrupted, leaving both fast and sustained components of release severely impaired for all subsequent stimuli.

Despite the dramatic loss of synaptic release, photodamage to the ribbons in bipolar cells was not accompanied by changes in ribbon number or the number of vesicles docked at the base of the ribbon, suggesting a role upstream of the final step in exocytosis, but downstream of vesicle delivery to the ribbon. Goldfish bipolar cells loaded with ATP-γS [29,30] can release a single pool of vesicles approximately equal in size to the pool of vesicles residing on ribbons, without diminishing the number of vesicles on the ribbon observed using electron microscopy, leading to the hypothesis that ATP is required for the priming of vesicles on the ribbon. By analogy, a disruption in the process of molecularly primed release-ready vesicles finding their way to sites in close proximity to calcium

Author Manuscript Author Manuscript Author Manuscript Author Manuscript

channels would account for many of the results we describe here and is an attractive model to describe our results.

Although the molecules being disrupted in our experiment are not known for certain, several possibilities can be considered. Free radicals generated by photobleaching almost certainly damage ribeye itself, as evidenced by the loss of binding to the fluorescent peptide, but other nearby proteins might also be damaged as well. From a molecular standpoint, vesicle priming involves the partial pre-assembly of SNARE proteins into position for rapid release, a process that has implicated several accessory proteins, including munc-13, munc-18 and RIM1 and RIM2 [31]. Of particular note, RIM2 and munc-13 are found near the base of the ribbon where the immediately releasable vesicles are thought to reside and RIM1 is located along the length of the ribbon, near ribeye[32].

Consistent with a role for the ribbon in preparing vesicles for rapid release, genetic mutation of the active zone protein bassoon, which causes synaptic ribbons to become unanchored from the membrane[4,33], results in the loss of synchronous release from the hair cell ribbon synapse[4] and some disruption of continuous release[34]. The effects of bassoon disruption on synaptic release, while consistent with a role for the ribbon in establishing a fast-releasing pool of vesicles and supporting continuous release, are complicated by the effect of bassoon disruption on calcium channel number, location and open-probability [34]. Unlike the bassoon mutant animals, which exhibited profound defects in fast synchronous release with much more subtle effects on continuous release[4], our results show that ribbon ablation initially leaves intact a population of vesicles, for which the synaptic ribbon had already primed for release, while preventing new vesicles from becoming release-ready. Based on these results, we suggest that the synaptic ribbon does more than position vesicles in a timely fashion, but also plays an active role in preparing vesicles for exocytosis. Moreover, our results establish a role for the ribbon in maintaining continuous release during prolonged stimuli.

Our results also argue against significant contribution for extra-ribbon release between rod bipolar cells and AII amacrine cells and between cones and off-bipolar cells or horizontal cells. Previous data indicate that exocytosis can occur at locations outside of the synaptic ribbon in rod bipolar cells of goldfish and in mouse hair cells [4,35-38]. Moreover, apparent conventional and other non-ribbon type synapses have been described in bipolar cells of several species [37,39-42]. However, synaptic release from bipolar cells requires high concentrations of calcium[43] and close proximity to calcium channels[15,22,44], which are mostly clustered near synaptic ribbons[8]. Similarly, photoreceptors exhibit vesicles closely positioned to the plasma-membrane and a relatively high-affinity calcium sensor for release[45], suggestive of the possibility of extra-ribbon release. Extra-ribbon release, when it has been observed, has been associated with the slower, sustained component of release. However, the role extra-ribbon release plays in synaptic communication remains unknown. In this study, we show that photodamage to the ribbon severely reduced both kinetic components and that the residual release after photobleach was sensitive to a second exposure to light, consistent with a requirement for a functional ribbon for both fast and slow components of release.

Author Manuscript Author Manuscript Author Manuscript Author Manuscript

Methods

Mouse Retinal Slice Preparation and solutions

Retinal slices were prepared from 4-6 week old C57/BL6 mice (Charles River). All procedures were approved by the Yale University Animal Care and Use Committee. Mice were anaesthetized with halothane (Sigma), sacrificed by cervical dislocation, and their eyes removed and enucleated. Whole retinas were isolated and placed on a 0.45 micron cellulose acetate/nitrate membrane filter (Millipore), which was secured with vacuum grease to a glass slide adjacent to the recording chamber. Slices were cut to a thickness of 150 μm using a tissue slicer, and transferred to the recording chamber while remaining submerged. The recording chamber was immediately attached to a perfusion system, and the slices were perfused at a rate of 5 ml/minute with Ames media bubbled with 95% O_2 and 5% CO_2. The Ames media was supplemented with 100 μM picrotoxin and 50 μM 1, 2, 5, 6-Tetrahydropyridin-4yl methylphosphinic acid (TPMPA) to block $GABA_A$ and $GABA_C$ receptors, 10 μM strychnine to block glycine receptors and 4uM L-AP4 to silence On bipolar cells. The standard recording solution for rod bipolar cells was composed of (in mM): 108 gluconic acid, 2 EGTA, 10 CsCl, 10 TEA, 4 MgATP, 1LiGTP. For photo bleaching experiments, 1 mM of the free radical scavenger glutathione was included in the recording solution. The amacrine cell internal solution was composed of (in mM): 100 $CsCH_3SO_3$, 10 EGTA, 20 TEA, 10 HEPES, 4 MgATP. 2 mM QX314 was added to block action potentials. The pH was adjusted to 7.4 with CsOH. The osmolarity of both extracellular and intracellular solutions was 289-293, with a pH of 7.35–7.40. All chemicals were obtained from Sigma, except for L-AP4, TPMPA (Tocris) and ribbon-binding peptides (New England Peptide). Glutathione was stored as a powder at 4°C, and was added to the pipette solution immediately before use. L-AP4 was stored as a stock solution at 4°C and was added to the bath solution at the day of experimentation. All other drugs were aliquoted, stored at -20°C, and dissolved in the pipette solution on the day of use.

Dissociation of mouse retinal bipolar cells and solutions

Retinas were isolated as described above, and cut into 4 pieces each. The retinal pieces were digested in a non-oxygenated AMES solution containing 1mg/mL cysteine and 40 mg/mL papain. After 35 min the retinal pieces were thoroughly washed using oxygenated Ames media, and gently triturated using a fire polished glass pipette. The dissociated preparation was plated onto Aclar bottomed recording chambers filled with oxygenated Ames media, and allowed to settle for 10 minutes before perfusion started. After the completion of an experiment, the preparation was immediately fixed in the recording chamber using 2.5% glutaraldehyde and 2.5% paraformaldehyde in phosphate buffer. Fixation then proceeded as previously described[46]. The experimental cell was located using a Nikon inverted microscope (TE300), and its location marked in the Aclar with a syringe needle for identification during EM sectioning. Photographs of the cell and surrounding area were taken to guide subsequent EM imaging.

Electrophysiology and analysis

Patch pipettes of resistance 8-11 MΩ were fabricated from borosilicate glass (TWF150-4, WPI) using a two-stage vertical puller (Narishige). Pipettes were coated with Sticky Wax,

Author Manuscript Author Manuscript Author Manuscript Author Manuscript

(Kerr Corp). Whole-cell recordings were obtained using a dual EPC10 amplifier (HEKA Instruments). The input/series resistances of the RBC and AII amacrine cell recordings were approximately 3 GΩ/15-20 MΩ, and 1 GΩ/20-25 MΩ, respectively. Cells were discarded if the series resistance exceeded 40 MΩ, or if the holding current changed suddenly. Holding potentials were corrected for the liquid junction potential, which was measured to be approximately −12 mV depending on solutions. Slices were viewed with a Zeiss Axioskop 2FS plus equipped with a water-immersion 40× DIC objective. Rod bipolar and AII amacrine cells were identified by their shape and position in the slice, as determined by fluorescent imaging. Photobleaching was performed using X-Cite 120Q (EXFO, Ontario, Canada) with a 488 nm band pass excitation filter (Chroma). Images were captured and stored with a CCD camera (Hamamatsu Orca II ER) acquired using MetaMorph acquisition software. Data were acquired using PatchMaster (HEKA Instruments), and analysis performed using Igor Pro (WaveMetrics), Kaleidagraph (Synergy Software), Origin (Microcal), and MiniAnalysis (Synaptosoft). Currents were elicited at 60 second intervals, collected at 20 kHz, and low-pass filtered at 1 kHz. Rod bipolar cell calcium currents were leak subtracted using a p/4 protocol. Statistical significance was determined using a Student's t test, with *, # and & indicating $p<0.002$. Errors represent S.E.M throughout the manuscript.

Fluorescent spot intensity for Figure 1 was measured by measuring an average fluorescence intensity in a 1 μm diameter circular region encompassing each ribbon spot. Surrounding each ribbon spot, a region containing no fluorescence spots was drawn and used to estimate the local background and subtracted from each spot.

To test the recovery after photobleaching, bipolar cells loaded with 20 μM fluorescein-conjugated peptide were subjected to 5 step depolarizations to 0 mV for 100 ms, then exposed to photobleaching light. Next, the cell was depolarized 5 times at 30 second intervals to deplete the photobleach sensitive pool and then again after 5 minute delay to look for recovery.

Salamander retinal slice recordings—Aquatic tiger salamanders (*Ambystoma tigrinum*, Kons Scientific, Germantown, WI) 18-25 cm in length were handled humanely according to protocols approved by the Institutional Animal Care and Use Committee at the University of Nebraska Medical Center. The salamander was decapitated with heavy shears, the cranium hemisected, and the spinal cord rapidly pithed. Animals were kept on a 12 hr. light/dark cycle and sacrificed 1-2 hrs. after the beginning of subjective night. After enucleation, the front of the eye, including the lens, was removed. The resulting eyecup was cut into thirds and a section was placed vitreal side down on a piece of filter paper (2 × 5 mm, Type AAWP, 0.8 μm pores, Millipore, Bedford, MA). After adhering to the filter paper, the retina was isolated under chilled amphibian superfusate. The retina and filter paper were cut into 125 μm slices using a razor blade (#121-6, Ted Pella Inc., Redding, CA) tissue chopper (Stoelting, Wood Dale, IL). Retinal slices were rotated 90° to permit viewing of the retinal layers when placed under a water immersion objective (60×, 1.0 NA) on an upright fixed stage microscope (Nikon E600FN, Tokyo, Japan). Slices were superfused at ∼1 ml/min with an oxygenated solution containing (in mM): 111 NaCl, 2.5 KCl, 2 $CaCl_2$,

Author Manuscript Author Manuscript Author Manuscript Author Manuscript

0.5 $MgCl_2$, 10 *N*-2-hydroxyethylpiperazine-*N*′ 2-ethanesulfonic acid (HEPES), 5 glucose (pH 7.8).

Cones were voltage clamped simultaneously with adjacent post-synaptic horizontal or OFF bipolar cells using an Axopatch 200B (Molecular Devices, Sunnyvale, CA) and Optopatch (Cairn Research, Faversham, UK) patch-clamp amplifiers. Recording pipettes were positioned with Huxley-Wall micromanipulators (Sutter Instruments, Novato, CA). Currents were low pass filtered at 2 kHz and acquired using a Digidata 1322 interface and pClamp 9.2 software (Molecular Devices). Acceptable access resistances were considered to be <50 MΩ.

Patch pipettes were pulled on a PP-830 vertical puller (Narishige USA, East Meadow, NY) from borosilicate glass pipettes (1.2 mm O.D., 0.9 mm I.D., with internal filament, World Precision Instruments, Sarasota, FL) and had tips of ∼1 μm O.D. with resistance values of 10 to 15 MΩ. The presynaptic recording pipette was filled with a solution containing: 40 mM CsGlutamate, 50 mM CsGluconate, 9.4 mM TEACl, 3.5 mM NaCl, 1 mM $CaCl_2$, 1 mM $MgCl_2$, 9.4 mM MgATP, 0.5 mM GTP, 5 mM EGTA, 10 mM HEPES (pH 7.2). For photo bleaching experiments, the peptide (40 μM) was added to this solution along with the anti-oxidants, reduced glutathione (1 mM) and 6-hydroxy-2,5,7,8-tetramethylchroman-2-carboxylic acid (Trolox, 1 mM). Post-synaptic pipettes were filled with a solution containing (in mM): 48 CsGluconate, 42 CsCl, 9.4 TEACl, 1.9 mM $MgCl_2$, 9.4 mM MgATP, 0.5 mM GTP, 5 mM EGTA, 32.9 mM HEPES (pH 7.2).

Confocal images were acquired using a laser confocal scanhead (Perkin Elmer Ultraview LCI) equipped with a cooled CCD camera (Orca ER). Bleaching was done using 488 nm light from an argon/krypton laser.

For capacitance recordings from cones, pipettes were coated with dental wax to reduce stray capacitance. Cell capacitance and residual pipette capacitance were compensated electronically. Capacitance measurements were made using the “track-in” mode of the Optopatch (Cairn Research, Faversham, UK) patch clamp amplifier [27,47]. The holding potential was varied sinusoidally (500-600 Hz, 30 mV peak to peak) about a holding potential of −70 mV. The peak amplitude of the capacitance increase was measured 30 ms after the end of the test step to avoid gating charges and allow time for the phase angle feedback circuitry to settle.

Electron microscopy—After fixation and dehydration in the recording chamber, recorded bipolar cells attached to Aclar were embedded in Embed 812, and the Aclar sheet was peeled away, leaving the cell at the surface of the block. Starting with the first section from the block face, 15-62 consecutive thin sections (80-90 nm) were collected, and the recorded neuron was located in EM based on the distinctive cell morphology and nearby landmarks from other cell types and debris. Images were then taken at 15,000-40,000× total magnification using a JEOL 1200 electron microscope.

Supplementary Material

Refer to Web version on PubMed Central for supplementary material.

Author Manuscript Author Manuscript Author Manuscript Author Manuscript

Acknowledgments

This work was funded by NIH grant R01EY003821 (GM), R01 EY000785, EY018111 (DZ) and EY10542 (WT) and Research to Prevent Blindness (WT). The authors would like to thank SueAnn Mentone for electron microscopy.

References

1. Cowan, WM.; Sudhof, TC.; Stevens, CF. Synapses. Johns Hopkins University Press; Baltimore, MD: 2001.
2. LoGiudice L, Matthews G. The role of ribbons at sensory synapses. Neuroscientist. 2009; 15:380–91. [PubMed: 19264728]
3. Lenzi D, von Gersdorff H. Structure suggests function: the case for synaptic ribbons as exocytotic nanomachines. Bioessays. 2001; 23:831–40. [PubMed: 11536295]
4. Khimich D, et al. Hair cell synaptic ribbons are essential for synchronous auditory signalling. Nature. 2005; 434:889–94. [PubMed: 15829963]
5. Davis GW, Bezprozvanny I. Maintaining the stability of neural function: a homeostatic hypothesis. Annu Rev Physiol. 2001; 63:847–69. [PubMed: 11181978]
6. Surrey T, et al. Chromophore-assisted light inactivation and self-organization of microtubules and motors. Proc Natl Acad Sci U S A. 1998; 95:4293–8. [PubMed: 9539730]
7. Hoffman-Kim D, Diefenbach TJ, Eustace BK, Jay DG. Chromophore-assisted laser inactivation. Methods Cell Biol. 2007; 82:335–54. [PubMed: 17586263]
8. Zenisek D, Horst NK, Merrifield C, Sterling P, Matthews G. Visualizing synaptic ribbons in the living cell. J Neurosci. 2004; 24:9752–9. [PubMed: 15525760]
9. Frank T, Khimich D, Neef A, Moser T. Mechanisms contributing to synaptic Ca2+ signals and their heterogeneity in hair cells. Proc Natl Acad Sci U S A. 2009; 106:4483–8. [PubMed: 19246382]
10. LoGiudice L, Sterling P, Matthews G. Mobility and turnover of vesicles at the synaptic ribbon. J Neurosci. 2008; 28:3150–8. [PubMed: 18354018]
11. Bartoletti TM, Babai N, Thoreson WB. Vesicle pool size at the salamander cone ribbon synapse. J Neurophysiol. 2010; 103:419–23. [PubMed: 19923246]
12. Choi SY, Jackman S, Thoreson WB, Kramer RH. Light regulation of Ca2+ in the cone photoreceptor synaptic terminal. Vis Neurosci. 2008; 25:693–700. [PubMed: 19112656]
13. Singer JH, Lassova L, Vardi N, Diamond JS. Coordinated multivesicular release at a mammalian ribbon synapse. Nat Neurosci. 2004; 7:826–33. [PubMed: 15235608]
14. Tsukamoto Y, Morigiwa K, Ueda M, Sterling P. Microcircuits for night vision in mouse retina. J Neurosci. 2001; 21:8616–23. [PubMed: 11606649]
15. Singer JH, Diamond JS. Sustained Ca2+ entry elicits transient postsynaptic currents at a retinal ribbon synapse. J Neurosci. 2003; 23:10923–33. [PubMed: 14645488]
16. Snellman J, Zenisek D, Nawy S. Switching between transient and sustained signalling at the rod bipolar-AII amacrine cell synapse of the mouse retina. J Physiol. 2009; 587:2443–55. [PubMed: 19332496]
17. Morkve SH, Veruki ML, Hartveit E. Functional characteristics of non-NMDA-type ionotropic glutamate receptor channels in AII amacrine cells in rat retina. J Physiol. 2002; 542:147–65. [PubMed: 12096058]
18. Veruki ML, Morkve SH, Hartveit E. Functional properties of spontaneous EPSCs and non-NMDA receptors in rod amacrine (AII) cells in the rat retina. J Physiol. 2003; 549:759–74. [PubMed: 12702738]
19. von Gersdorff H, Vardi E, Matthews G, Sterling P. Evidence that vesicles on the synaptic ribbon of retinal bipolar neurons can be rapidly released. Neuron. 1996; 16:1221–7. [PubMed: 8663998]
20. Veruki ML, Morkve SH, Hartveit E. Activation of a presynaptic glutamate transporter regulates synaptic transmission through electrical signaling. Nat Neurosci. 2006; 9:1388–96. [PubMed: 17041592]

Author Manuscript Author Manuscript Author Manuscript Author Manuscript

21. Palmer MJ, Hull C, Vigh J, von Gersdorff H. Synaptic cleft acidification and modulation of short-term depression by exocytosed protons in retinal bipolar cells. J Neurosci. 2003; 23:11332–41. [PubMed: 14672997]
22. Jarsky T, Tian M, Singer JH. Nanodomain control of exocytosis is responsible for the signaling capability of a retinal ribbon synapse. J Neurosci. 2010; 30:11885–95. [PubMed: 20826653]
23. DeVries SH. Exocytosed protons feedback to suppress the Ca2+ current in mammalian cone photoreceptors. Neuron. 2001; 32:1107–17. [PubMed: 11754841]
24. Molloy DP, et al. Structural determinants present in the C-terminal binding protein binding site of adenovirus early region 1A proteins. J Biol Chem. 1998; 273:20867–76. [PubMed: 9694833]
25. Schmitz F, Konigstorfer A, Sudhof TC. RIBEYE, a component of synaptic ribbons: a protein's journey through evolution provides insight into synaptic ribbon function. Neuron. 2000; 28:857–72. [PubMed: 11163272]
26. Bonazzi M, et al. CtBP3/BARS drives membrane fission in dynamin-independent transport pathways. Nat Cell Biol. 2005; 7:570–80. [PubMed: 15880102]
27. Rabl K, Cadetti L, Thoreson WB. Kinetics of exocytosis is faster in cones than in rods. J Neurosci. 2005; 25:4633–40. [PubMed: 15872111]
28. Singer JH, Diamond JS. Vesicle depletion and synaptic depression at a mammalian ribbon synapse. J Neurophysiol. 2006; 95:3191–8. [PubMed: 16452253]
29. Heidelberger R. Adenosine triphosphate and the late steps in calcium-dependent exocytosis at a ribbon synapse. J Gen Physiol. 1998; 111:225–41. [PubMed: 9450941]
30. Heidelberger R, Sterling P, Matthews G. Roles of ATP in depletion and replenishment of the releasable pool of synaptic vesicles. J Neurophysiol. 2002; 88:98–106. [PubMed: 12091535]
31. Rizo J, Rosenmund C. Synaptic vesicle fusion. Nat Struct Mol Biol. 2008; 15:665–74. [PubMed: 18618940]
32. tom Dieck S, et al. Molecular dissection of the photoreceptor ribbon synapse: physical interaction of Bassoon and RIBEYE is essential for the assembly of the ribbon complex. J Cell Biol. 2005; 168:825–36. [PubMed: 15728193]
33. Dick O, et al. The presynaptic active zone protein bassoon is essential for photoreceptor ribbon synapse formation in the retina. Neuron. 2003; 37:775–86. [PubMed: 12628168]
34. Frank T, et al. Bassoon and the synaptic ribbon organize Ca(2)+ channels and vesicles to add release sites and promote refilling. Neuron. 2010; 68:724–38. [PubMed: 21092861]
35. Zenisek D, Steyer JA, Almers W. Transport, capture and exocytosis of single synaptic vesicles at active zones. Nature. 2000; 406:849–54. [PubMed: 10972279]
36. Zenisek D. Vesicle association and exocytosis at ribbon and extraribbon sites in retinal bipolar cell presynaptic terminals. Proc Natl Acad Sci U S A. 2008; 105:4922–7. [PubMed: 18339810]
37. Midorikawa M, Tsukamoto Y, Berglund K, Ishii M, Tachibana M. Different roles of ribbon-associated and ribbon-free active zones in retinal bipolar cells. Nat Neurosci. 2007; 10:1268–76. [PubMed: 17828257]
38. Coggins MR, Grabner CP, Almers W, Zenisek D. Stimulated exocytosis of endosomes in goldfish retinal bipolar neurons. J Physiol. 2007; 584:853–65. [PubMed: 17823206]
39. Miller RF, Gottesman J, Henderson D, Sikora M, Kolb H. Pre- and postsynaptic mechanisms of spontaneous, excitatory postsynaptic currents in the salamander retina. Prog Brain Res. 2001; 131:241–53. [PubMed: 11420944]
40. Wong-Riley MT. Synaptic orgnization of the inner plexiform layer in the retina of the tiger salamander. J Neurocytol. 1974; 3:1–33. [PubMed: 4132946]
41. Grunert U, Haverkamp S, Fletcher EL, Wassle H. Synaptic distribution of ionotropic glutamate receptors in the inner plexiform layer of the primate retina. J Comp Neurol. 2002; 447:138–51. [PubMed: 11977117]
42. Hull C, Studholme K, Yazulla S, von Gersdorff H. Diurnal changes in exocytosis and the number of synaptic ribbons at active zones of an ON-type bipolar cell terminal. J Neurophysiol. 2006; 96:2025–33. [PubMed: 16738212]
43. Heidelberger R, Heinemann C, Neher E, Matthews G. Calcium dependence of the rate of exocytosis in a synaptic terminal. Nature. 1994; 371:513–5. [PubMed: 7935764]

Author Manuscript Author Manuscript Author Manuscript Author Manuscript

44. von Gersdorff H, Matthews G. Dynamics of synaptic vesicle fusion and membrane retrieval in synaptic terminals. Nature. 1994; 367:735–9. [PubMed: 7906397]

45. Thoreson WB, Rabl K, Townes-Anderson E, Heidelberger R. A highly Ca2+-sensitive pool of vesicles contributes to linearity at the rod photoreceptor ribbon synapse. Neuron. 2004; 42:595–605. [PubMed: 15157421]

46. Paillart C, Li J, Matthews G, Sterling P. Endocytosis and vesicle recycling at a ribbon synapse. J Neurosci. 2003; 23:4092–9. [PubMed: 12764096]

47. Johnson SL, Thomas MV, Kros CJ. Membrane capacitance measurement using patch clamp with integrated self-balancing lock-in amplifier. Pflugers Arch. 2002; 443:653–63. [PubMed: 11907834]

Author Manuscript Author Manuscript Author Manuscript Author Manuscript

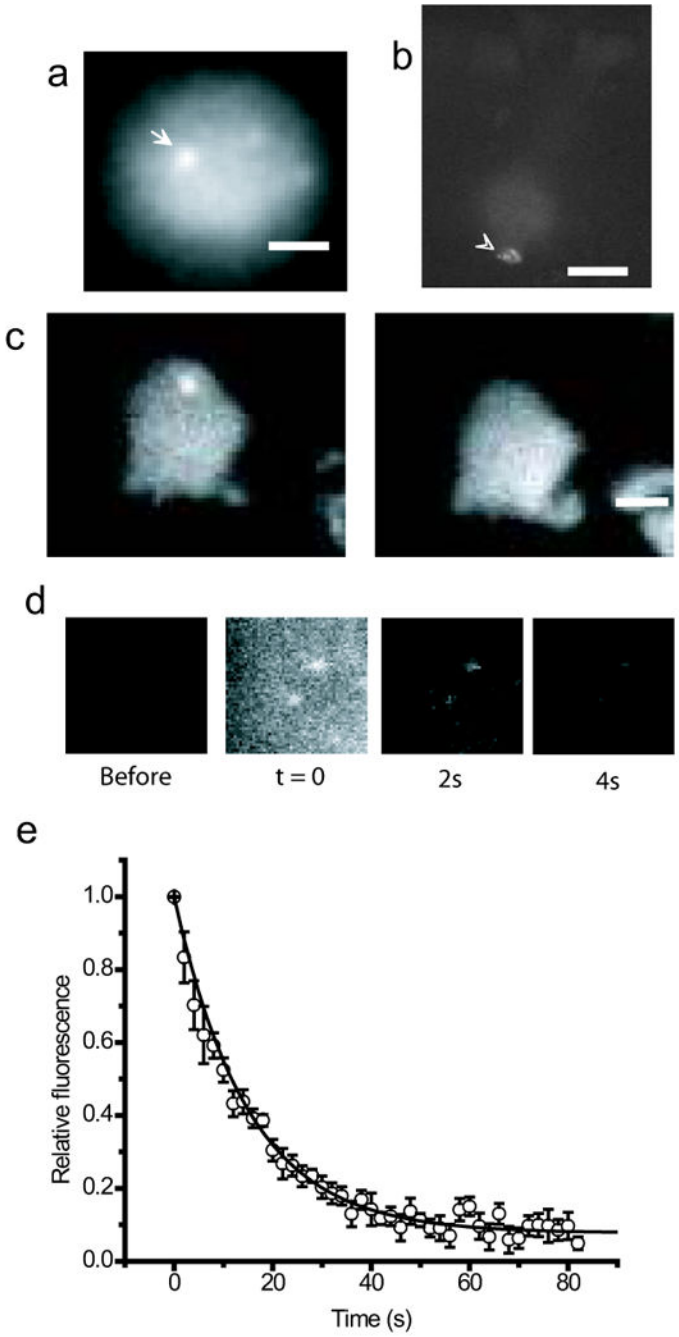

Figure 1.

A synaptic ribbon-binding peptide exhibits irreversible photobleaching. **a.** Fluorescent image of synaptic terminal of mouse retinal bipolar cell loaded with fluorescein-conjugated ribbon binding peptide. Note the spots representing peptide binding to the synaptic ribbon[8,10]. Scale bar = 1 μm. **b.** Confocal image of salamander cone photoreceptor loaded with HyLite-488 conjugated ribbon-binding peptide in a retinal slice. Arrows denote location of ribbons. Scale bar = 10 μm. **c.** (left) Image of bipolar cell loaded with the fluorescein-conjugated peptide. **c**. (right) the same terminal as in **c** (left), 150 seconds after

Author Manuscript Author Manuscript Author Manuscript Author Manuscript

exposure to 15 seconds of 488 nm light. Note that the fluorescence within the terminal returns to pre-bleach levels, but the ribbon fluorescence does not recover. **d.** Time series of epifluorescence images of permeabilized mouse bipolar cells superfused with ribbon-binding peptide. Mouse bipolar cells permeabilized with β-escin were superfused with a solution containing 50 μM HyLite488 conjugated peptide. Series of images shows fluorescence immediately before (left), at the end of a 5 second application of the peptide (t = 0 s) and 2 and 4 seconds after washing with dye free solution. Each image is 4.3 μm wide. **e**. Measurement of peptide unbinding from the ribbon. The average fluorescence intensity in a circular region encompassing each ribbon spot was measured for each time point (n = 10 ribbons in 3 cells) after background subtraction. Spot intensities were normalized to the peak intensity and averaged over time. Error bars represent S.E.M. Solid line represents best-fit exponential curve through the points.

Author Manuscript
Author Manuscript
Author Manuscript
Author Manuscript

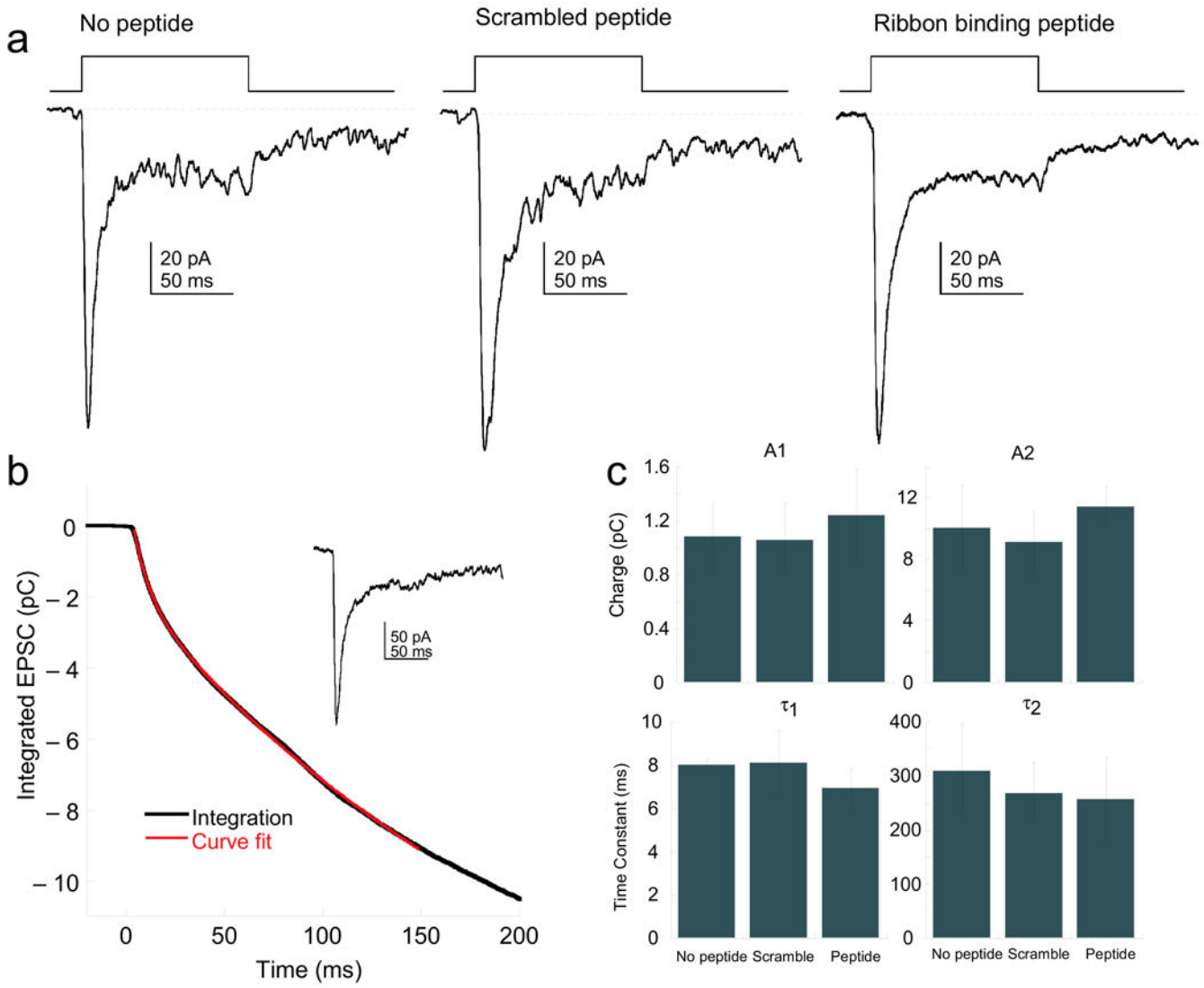

Figure 2.

Ribbon binding peptide has no effect on synaptic transmission. Rod bipolar cells and AII amacrine cells were simultaneously whole-cell voltage clamped. Step depolarizations to −10 or 0 mV for 100 ms elicited an inward calcium current in the presynaptic bipolar cell, which triggers an EPSC measured in a post-synaptic AII amacrine cell. **a**. Average EPSCs recorded from amacrine cells without peptide (left, n = 10), or with ribbon-binding peptide (right, n = 10). **b.** Time integral of an EPSC (inset) recorded from one amacrine bipolar cell pair in the presence of ribbon peptide, best fit to equation 1. **c.** Bar graphs showing average τ_1, τ_2, A_1, A_2 for synaptic responses without and with peptide. Without peptide: A_1 = 1.08 pC ± 0.24, A_2 = 10.0 pC ± 2.2, τ_1 = 8.02 ms ± 2.50, τ_2 = 309 ms ± 88. With peptide: A_1 = 1.24 pC ± 0.34, A_2 = 11.4 pC ± 5.0631, τ_1 = 7.0 ms ± 0.88746, τ_2 = 257 ms ± 78. Errors represent S.E.M.

Author Manuscript
Author Manuscript
Author Manuscript
Author Manuscript

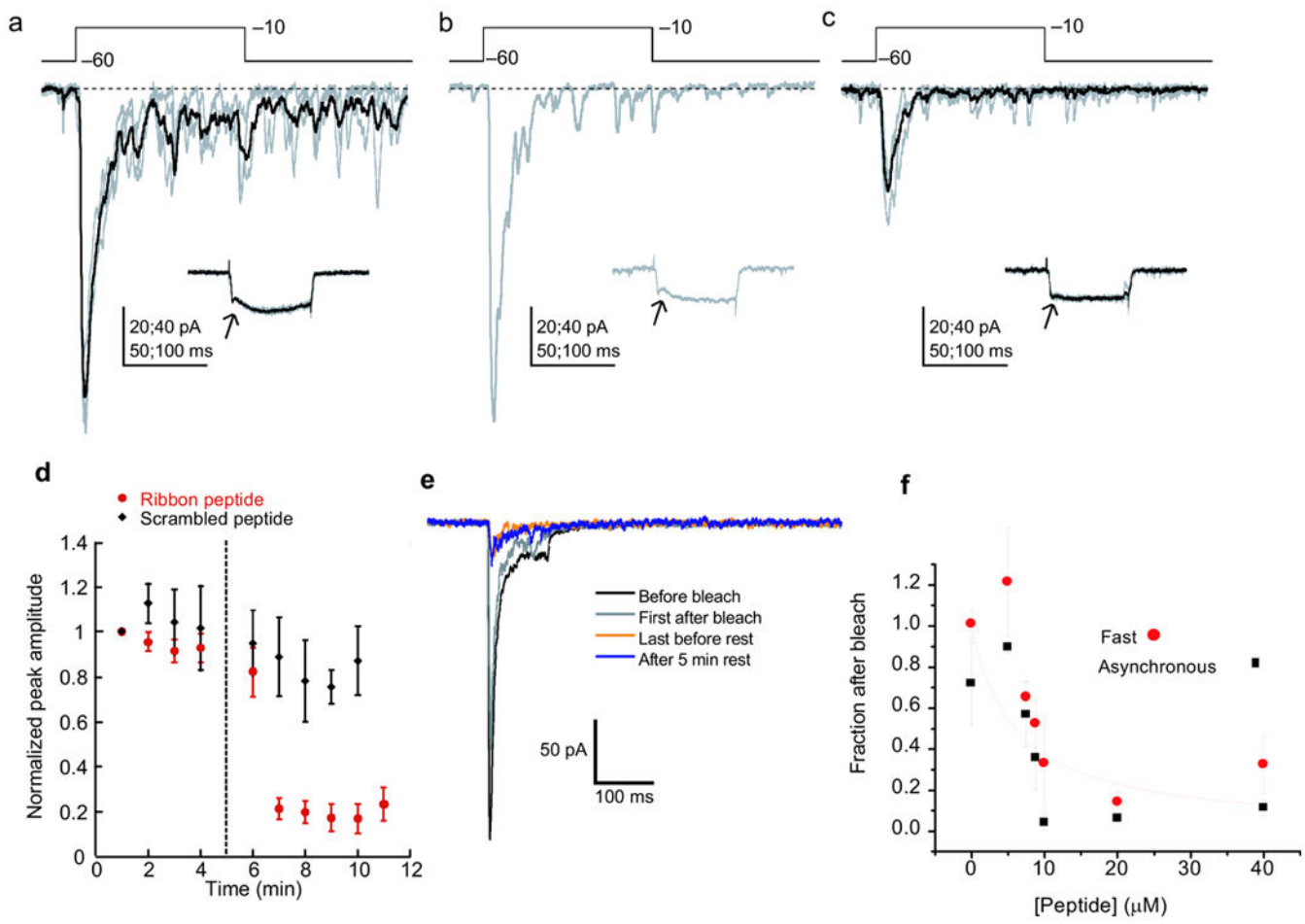

Figure 3.

Photodamage to the ribbon blocks replenishment of the immediately releasable pool in bipolar cell ribbon synapses. **a**–**c.** A series of EPSCs recorded from an AII amacrine – rod bipolar cell pair in the presence of 20 μM ribbon peptide. Gray: individual traces, black: average. AII EPSCs and the corresponding RBC calcium currents (insets) were recorded before photobleach (**a**), immediately after photobleach (**b**) and subsequently (**c**). Note that RBC current shows deviation from normal square wave expected for calcium current in (arrows), due to presynaptic glutamate transporter current in (**a**) and (**b**), but not in (**c**). **d**. Amplitude over time: The peak amplitude of EPSC from 20 pairs loaded with 10 – 20 μM ribbon peptide, and 6 pairs loaded with 40 μM scrambled peptide, were normalized, averaged and plotted as a function of time. Dashed line represents the time of the 15 s photobleach. **e.** EPSCs exhibit little recovery after longer delay. Synaptic responses recorded before (black), first after (gray) after 5 depolarizations after photobleach (orange) and after the 5-minute delay (blue) **f.** Relationship between peptide concentration and the peak of EPSC with photobleaching. The EPSC was recorded before and after photobleach, and the fraction of the peak response (after photobleach/ before photobleach) and delayed component was plotted as a function of peptide concentration. 5 μM, n = 3; 7.5 μM, n = 3; 10 μM, n = 5; 20 μM, n = 8; 40 μM, n = 10.. Solid red line shows best-fit line (Kd = 6.0 μM) through the peak responses assuming first-order binding.

Author Manuscript Author Manuscript Author Manuscript Author Manuscript

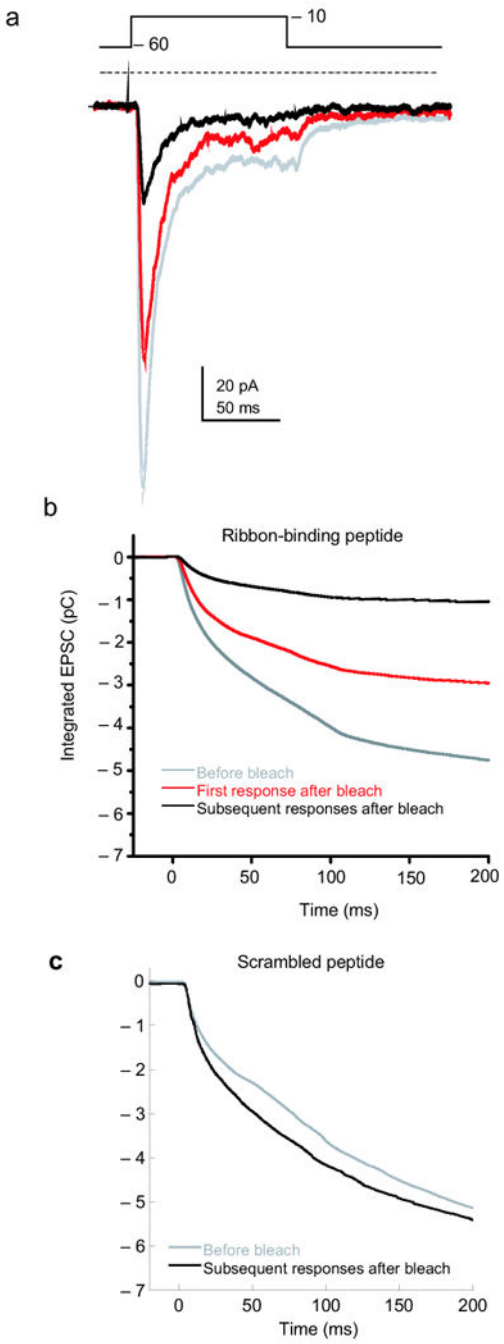

Figure 4.

Kinetic analysis of effects of photobleaching on AII postsynaptic response **a**. Overlay showing the averaged AII EPSCs in response to 100 ms steps to −10 mV before photobleach (grey), the trace immediately after photobleach (red), and the subsequent averaged traces (black) for one recorded pair. **b**. Integration of AII postsynaptic response to RBC voltage steps plotted over time before bleach (gray), first after bleach (red) and subsequent responses (black). Results show averages from 25 pairs loaded with 10 - 40 μM ribbon binding peptide and subjected to FALI. **c.** The average integrals of 6 pairs loaded with 40

Author Manuscript Author Manuscript Author Manuscript Author Manuscript

μM scrambled peptide and subjected to FALI, showing both before (gray) and after bleach and at least one voltage step (black).

Author Manuscript Author Manuscript Author Manuscript Author Manuscript

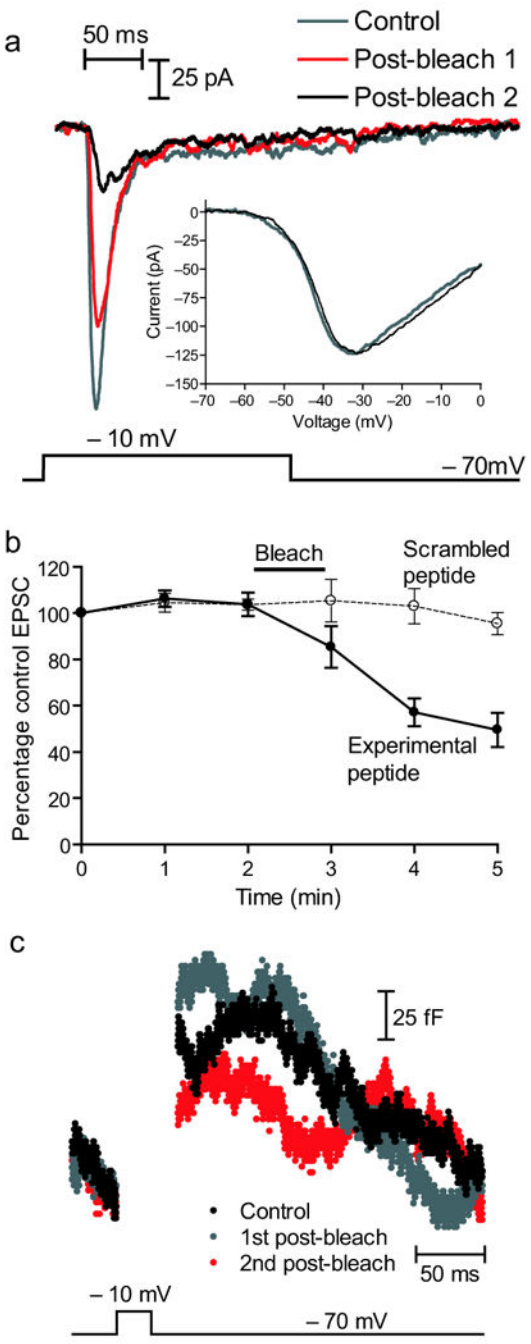

Figure 5.

Effects of acute damage to cone photoreceptor ribbons on synaptic transmission. **a.** A series of EPSCs recorded from a salamander off-bipolar cell in response to voltage steps to − 10 mV for 100 ms in the presynaptic cone before photobleach (gray), first after photobleach (red) and second response (black) after photobleach. **b.** Amplitude over time: The peak amplitude of EPSCs from horizontal or off-bipolar cells evoked by stimulation of cones loaded with 40 μM ribbon peptide (n=20 pairs) or 40 μM scrambled peptide (n=6 pairs). EPSC measurements were normalized, averaged and plotted as a function of time. **c.**

Author Manuscript Author Manuscript Author Manuscript Author Manuscript

Example of capacitance measurements taken from one cell in response to step depolarizations to −10 mV for 25 ms before photobleach (black), first response after photobleach (gray) and second response after photobleach (red). Photobleaching caused a reduction in the size of the capacitance jump, but no change in the rate of endocytosis. Errors represent S.E.M.

Author Manuscript Author Manuscript Author Manuscript Author Manuscript

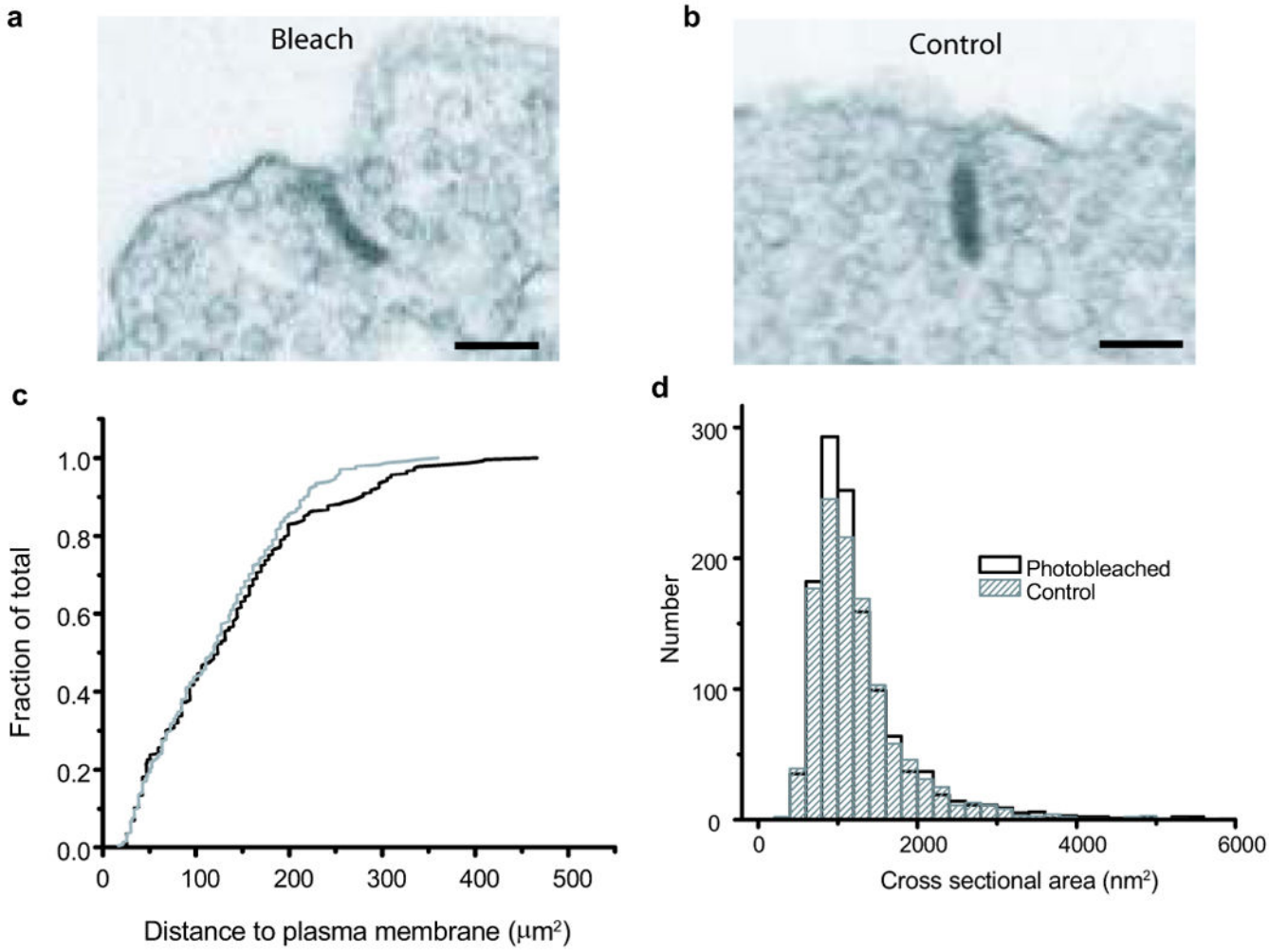

Figure 6.

EM **a**. electron micrograph of a ribbon from a cell subjected to photobleaching illumination followed by two depolarizations. Scale bar = 100 nm. **b.** electron micrograph of a ribbon in a control cell. Scale same as in **a. c**. cumulative histogram of distance of the centers of vesicles on ribbons adjacent to the plasma membrane for ribbons sections where ribbons were found adjacent to the plasma membrane for control (gray) and photobleached (black) cells. **d**. Histogram of the cross sectional areas of organelles found near the ribbon in control (gray hatched) and photo-bleached (black) retinal bipolar cells.